Shape-persistent, ruthenium(II)- and iron(II)-bisterpyridine metallodendrimers: synthesis, traveling-wave ion-mobility mass spectrometry, and photophysical properties

ARTICLE *in* NEW JOURNAL OF CHEMISTRY · JANUARY 2012

Impact Factor: 3.09 · DOI: 10.1039/C2NJ20799K

NJC

New Journal of Chemistry

A journal for new directions in chemistry

www.rsc.org/njc

Volume 36 | Number 2 | February 2012 | Pages 181–512

Themed issue: Dendrimers II

ISSN 1144-0546

RSC Publishing

COVER ARTICLE

Wesdemiotis and Newkome *et al.*
Shape-persistent ruthenium(II)- and iron(II)-bisterpyridine metallodendrimers

1144-0546(2012)36:2;1-I

NJC

Dynamic Article Links

Cite this: *New J. Chem.*, 2012, **36**, 484–491

www.rsc.org/njc

PAPER

Shape-persistent, ruthenium(II)- and iron(II)-bisterpyridine metallodendrimers: synthesis, traveling-wave ion-mobility mass spectrometry, and photophysical properties†

Jin-Liang Wang,[a] Xiaopeng Li,[ab] Carol D. Shreiner,[a] Xiaocun Lu,[a] Charles N. Moorefield,[a] Sreedhar R. Tummalapalli,[b] Douglas A. Medvetz,[b] Matthew J. Panzner,[b] Frank R. Fronczek,[c] Chrys Wesdemiotis*[ab] and George R. Newkome*[ab]

Received (in Montpellier, France) 15th September 2011, Accepted 15th December 2011
DOI: 10.1039/c2nj20799k

A class of shape-persistent metallodendrimer has been developed through a self-assembly strategy, in which ⟨tpy-Ru^{II}-tpy⟩ or ⟨tpy-Fe^{II}-tpy⟩ connectivity is utilized, as branching moieties or nodes. These metallomacromolecules were fully characterized by ^{1}H and ^{13}C NMR, traveling wave ion mobility mass spectrometry (TWIM MS), single crystal X-ray, UV-vis absorption, photoluminescence, and cyclic voltammetry. Significant increase in the drift times of the same charge states was observed with increasing generation of these complexes, which is in line with the change of molecular size. Moreover, the photophysical properties (molar extinction coefficients) and electrochemical stability of the complexes were noticeably different depending on size and metal ion center.

Introduction

Construction of highly ordered, 2D and 3D supramolecular architectures employing self-assembly strategies based on versatile building blocks has generated considerable attention over the past few decades.[1] One notable strategy is through ligand–metal–ligand coordination to construct interesting predesigned topologic architectures, including a variety of macrocycles,[2] cages or spheres,[3] prisms,[4] and dendrimers.[5] Among various types of self-assembled topologies, metallo-dendrimers are quite attractive due to their applications in catalysis, sensing, and light-harvesting.[6] Combination of various dyes or chromophores into nanosized, shape-persistent metallo-dendrimers and metallomacrocycles, formed by self-assembly methods, provides a platform to investigate energy or charge transfer processes, which are important requirements for prescreening their applications in spin crossover based on light-induced excited-state spin trapping[7] prevalent in transition metal complexes with electronic configuration d^4–d^7 as well as dye-sensitized solar cells and other light-harvesting devices.[7] Moreover, 2,2′:6′,2″-terpyridine (tpy) ligands have gained considerable utility in metal–ligand coordination chemistry because of the structural diversity available by using -⟨tpy-M^{II}-tpy⟩- connectivity; their relative ease to functionalize is also critical to tailoring multinuclear assemblies.[8] However, very few examples concerning their integration into different, easily accessible -⟨tpy-M^{II}-tpy⟩- spacers in shape-persistent metallodendrimers *via* self-assembly have been reported; due, in part, to the difficulties associated with the step-wise synthesis and separation of the desired heterometallic product(s) from similar by-products.[9] The characterization of such complicated metallodendrimers is also a challenge because it is not easy to obtain single crystals of such complex macrostructures, especially at higher generations. A combination of NMR spectroscopy and electrospray ionization (ESI) or matrix-assisted laser desorption ionization (MALDI) mass spectrometry (MS)[10] is typically utilized; however, construction of multinuclear assemblies always leads to some labile species (several counterions and reversible transition-metal complexes), which can easily generate numerous differently charged fragments and their isotope peaks tend to overlap in ESI MS. These problems obviously increase the difficulty in their precise structural identification.[11]

Recently, ion mobility spectroscopy-mass spectrometry (IMS MS) and traveling wave ion mobility mass spectrometry (TWIM MS) have been employed to detect and characterize complicated supramolecular species.[12] These techniques afford

[a] *Department of Polymer Science, The University of Akron, 302 Buchtel Common, Akron, OH 44325, USA. E-mail: newkome@uakron.edu; Fax: +1 330-972-2368*
[b] *Department of Chemistry, The University of Akron, 302 Buchtel Common, Akron, OH 44325, USA. E-mail: wesdemiotis@uakron.edu*
[c] *Department of Chemistry, Louisiana State University, Baton Rouge, LA 70803, USA*

† Electronic supplementary information (ESI) available. CCDC reference number 855619. For ESI and crystallographic data in CIF or other electronic format see DOI: 10.1039/c2nj20799k

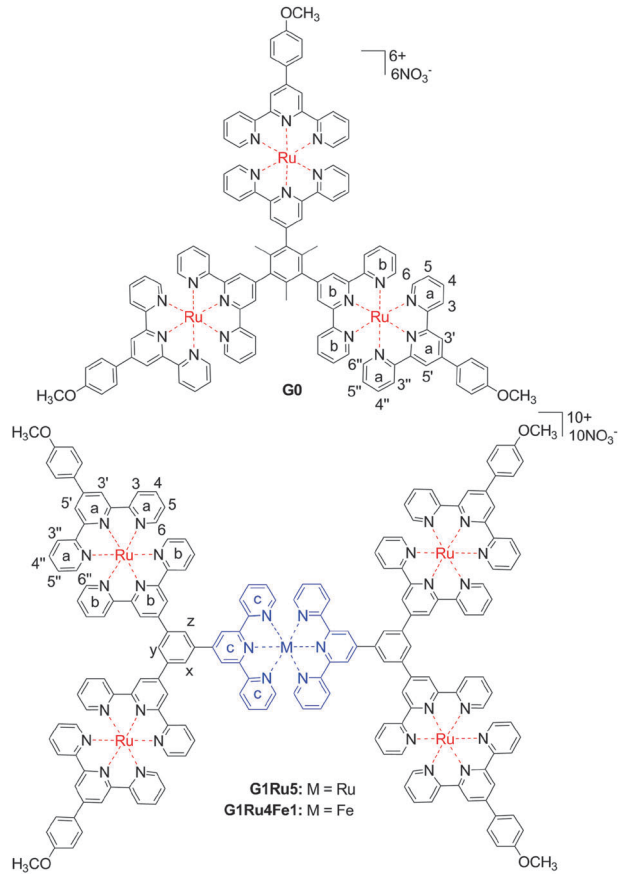

Fig. 1 Structures of the Ru^{II} core (**G0**) and Ru^{II}/Fe^{II} metallodendrimers.

possible avenues to separate related supramolecular species from fragments with the same mass-to-charge ratio (m/z) as well as isomeric architectures with similar charge.[13] The time needed for an ion to travel through the ion mobility region is defined as its drift time, which is affected by the mass, charge, and *shape* of the ions. This affords information about the *conformation and geometry of the drifting ions*.

Herein, we present the synthesis, *via* a self-assembly strategy, isolation, and structural characterization of a family of small shape-persistent metallodendrimers (Fig. 1), based on ⟨tpy-Ru^{II}-tpy⟩ or ⟨tpy-Fe^{II}-tpy⟩ connectivity, in the form of either the branch (**G0**) or core unit (**G1Ru5** and **G1Ru4Fe1**). These metallomacromolecules were identified by NMR, X-ray single crystal, TWIM MS, UV-vis absorption, photoluminescence, and cyclic voltammetry providing information about their purity, molecular size and shape, as well as their photophysical and electrochemical properties, which were notably modulated by dendron generation and metal ion center.

Results and discussion

Scheme 1 illustrates the synthetic approach to the complexes **G0**, in which the key core ligands, tris-terpyridine **T3** and **MT3** with three methyl groups, were prepared by condensing 2-acetylpyridine with either 1,3,5-triformylbenzene to generate **T3** or 1,3,5-triformyl-2,4,6-trimethylbenzene[14] for **MT3** under solvent-free basic conditions.[15] Each intermediate hexaketone was then treated with ammonium hydroxide to produce the desired tris-terpyridines in 31% and 25%, respectively. The paramagnetic,

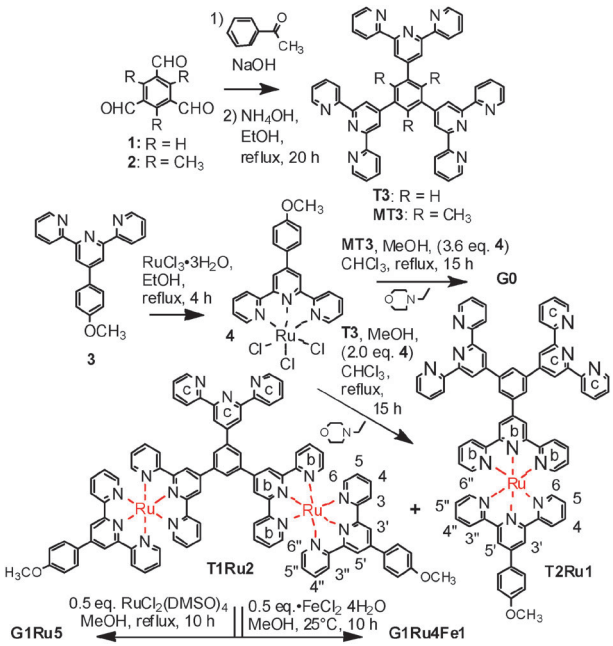

Scheme 1 Synthetic route to ligands **T3** and **MT3** along with the self-assembled metallomacromolecules.

Ru^{III} mono-capping adduct **4** was then obtained by refluxing a mixture of 4′-(*p*-methoxyphenyl)-2,2′ : 6′,2″-terpyridine (**3**) with $RuCl_3 \cdot 3H_2O$, according to the literature.[16] The trinuclear complex **G0** was obtained (52%) by reaction of **MT3** with 3.6 equiv. of adduct **4** in a mixture of MeOH and $CHCl_3$ in the presence of *N*-ethylmorpholine for 12 h under reflux conditions and the resultant crude product was column chromatographed (SiO_2) eluting with a solvent mixture of H_2O/MeCN/sat.KNO_3 (aq.) (1/12/1 (v/v/v)) to give the desired product **G0**, as a dark red solid.

The ^1H NMR spectrum of **MT3** revealed a diagnostic singlet at 1.96 ppm corresponding to a single type of methyl proton on the central mesitylene moiety, which was shifted downfield to 2.57 ppm in complex **G0** due to the lower electron density resulting from the coordination effect. Meanwhile, as shown in Fig. 2, ^1H NMR spectrum of **G0** revealed two sets of terpyridine resonances, consistent with the formation of the symmetric trinuclear complex. For example, two singlets for 3′,5′-tpy*H* were shifted downfield to 9.21 and 9.14 ppm in comparison with the peaks at 8.73 and 8.43 ppm, respectively. As expected, a dramatic upfield shift for the 6,6″ proton signal

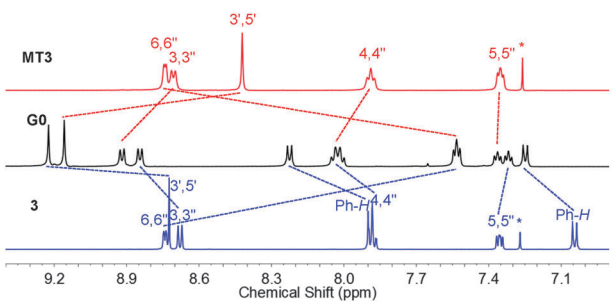

Fig. 2 Aromatic regions of the 500 MHz ^1H NMR spectra for ligands **MT3** and **3** (in $CDCl_3$) and complexes **G0** with NO_3^-, as the counterion (in $CD_3OD/CDCl_3$, 3/1).

occurred upon complexation due to the shielding effect of the perpendicular terpyridine counterpart with metal center. Moreover, two sharp peaks in the ^{13}C NMR spectrum are located at 56.1 (OCH_3) and 20.9 ppm (CH_3).

The key precursor for the next generation metallodendrimer is the dinuclear ruthenium complex **T1Ru2** possessing a free terpyridine segment, which failed to form when a simple 1 : 1 ratio of the core **T3** and the capping adduct **4** were utilized under typical reaction conditions;[9a] however, using a 1 : 2 ratio of **T3** with **4** led to the desired product. With this method, the dinuclear complexes **T1Ru2** were isolated (48%) after chromatography [SiO_2; H_2O/MeCN/sat.KNO_3(aq.), 1/15/1 (v/v/v)], while the mononuclear complex **T2Ru1** with two free terpyridine segments was obtained in 18% isolated yield using [H_2O/MeCN/sat.KNO_3(aq), 1/20/1 (v/v/v)], as eluent. These complexes are readily soluble in common organic solvents, such as $CHCl_3$, MeOH, and DMSO (with Cl^- or NO_3^-, as counterion) or MeCN and acetone (with PF_6^-, as counterion). The structure and purity of these dendrons were ascertained by ^1H and ^{13}C NMR, COSY, as well as MALDI-ToF/ESI MS. As shown in Fig. 3, in comparison with the two ligands, both **T1Ru2** and **T2Ru1** exhibit more complex NMR patterns with the expected downfield shifts due to the lower electron density resulting from the metal incorporation. Moreover, both complexes showed three diagnostic peaks for 3′,5′-tpy*H* (singlet) and 3,3′′-tpy*H*s (doublet) in a 1 : 1 : 2 or 2 : 2 : 1 ratio, respectively. Although the two dendrons exhibit a similar peak pattern for terpyridine, there are slight variations, especially for the *b* pyridine ring protons, which have a dramatic downfield shift (+0.14 ppm for ^{b}Py-$H^{3',5'}$) due to coordination, in which the 3′,5′-tpy*H* protons are particularly sensitive to their environment. Hence, it is a key discernable feature for structural identification in such similar structures. Meanwhile, the peaks for 6,6′′-tpy*H*s exhibited a dramatic upfield shift due to

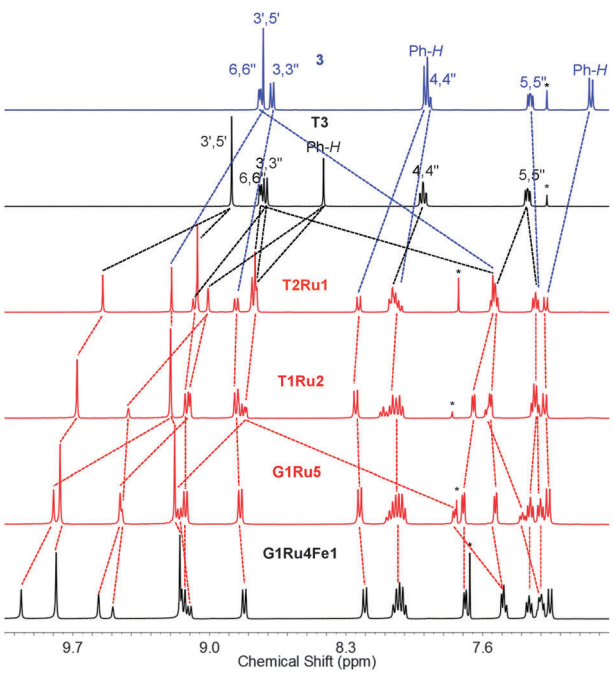

Fig. 3 Aromatic regions of the 500 MHz ^1H NMR spectra for ligands **T3** and **3** (in $CDCl_3$) and complexes **T2Ru1**, **T1Ru2**, **G1Ru5**, and **G1Ru4Fe1** with NO_3^-, as the counterion (in 3 : 1 $CD_3OD/CDCl_3$).

the shielding effect of metal centers relative to the uncomplexed parts. The singlets at 8.42 ppm (in the spectrum of **T3**) for protons of the central phenyl group showed successive downfield shifts and split into two types due to their environment; this is most noticeable for Ph-*H*, which shifts to 9.42 ppm in **T1Ru2**, and even higher than the one for the coordinated 3′,5′-tpy*H*.

The metallodendrimer **G1Ru5** (Scheme 1) was generated by refluxing a solution of **T1Ru2** and 0.50 equivalents of $RuCl_2(DMSO)_4$[17] in MeOH for 10 h followed by flash column chromatography (SiO_2) eluting with a H_2O/MeCN/sat.KNO_3(aq.) (1 : 8 : 1 v/v/v) mixture in 70% isolated yield. Meanwhile, the reaction of **T1Ru2** (Scheme 1) with 0.50 equivalents of $FeCl_2{\cdot}4H_2O$ in MeOH for 10 h gave (84%) the heteronuclear dendrimer **G1Ru4Fe1** after column chromatography (SiO_2) eluting with a solvent mixture of H_2O/MeCN/sat. KNO_3(aq.) (1 : 7 : 1, v/v/v). The ^1H NMR spectra of two dendrimers were assigned (Fig. 3) with the aid of 2D COSY spectra (see ESI†) revealing three sets of diagnostic absorptions for coordinated 3′,5′-tpy*H*s (singlet), 3,3′′-tpy*H*s (doublet), and 6,6′′-tpy*H*s (doublet) in a 2 : 2 : 1 ratio, respectively. In comparison with the free terpyridine protons in **T1Ru2**, the protons in **G1Ru5** have an obvious downfield shift that is even lower than the other two coordinated terpyridines. Moreover, when the central metal ion was changed from Ru(II) to Fe(II), the 3′,5′-tpy*H* of **G1Ru4Fe1** showed distinct downfield shifts relative to the same protons in the **G1Ru$_5$**, which resulted from enhanced electron deficiency by ⟨tpy-Fe^{II}-tpy⟩ connectivity. Notably, the protons belonging to the central positions in **G1Ru4Fe1** showed an upfield shift compared with those in **G1Ru5**. The ^{13}C NMR spectra of these dendrimers were also in full agreement with their symmetry resulting in the observation of three peaks for 3′,5′-tpy*C*s (see ESI†).

In addition to NMR, MALDI-ToF and ESI MS coupled with traveling wave ion mobility (TWIM) mass spectrometry were applied to further verify the structures and purity of the desired complexes.[13] Both MALDI-ToF MS and ESI MS of these metallodendrimers with NO_3^- counterions generated a significant number of fragments (spectra not shown). In order to obtain more informative mass spectra for identification of the structure and purity of the dendrons, the NO_3^- salts were converted to the corresponding PF_6^- salts, which produce sharp molecular ion patterns with few fragments (Fig. 4, Fig. S1 and S2, ESI†). For example, the structure and purity of **G0** are further corroborated by the two intense MALDI-ToF MS peaks (Fig. S4, ESI†) at m/z 2860.8 $(M - PF_6)^+$ (calcd m/z = 2861.3) and 1358.4 $(M - 2PF_6)^{2+}$ (calcd m/z = 1358.2); similarly, the MALDI-ToF mass spectrum of **G1Ru5** displays a sharp molecular ion peak at 4712.7 $(M - PF_6)^+$ (calcd m/z = 4713.3) and a +2 charge state signal at 2283.8 $(M - 2PF_6)^{2+}$ (calcd m/z = 2284.1). In contrast, MALDI peaks for intact **G1Ru4Fe1** were not detected due to the lower inherent stability of the ⟨tpy-Fe^{II}-tpy⟩ connectivity.[13d] These assembled complexes were, however, confirmed by ESI MS, which is a milder analytical MS procedure. As mentioned above, coordinatively bound self-assemblies carrying neutral ligands are ionized to intact supramolecular ions by removal of one or more of their counterions. ESI MS of these complexes led to supramolecular ions missing 1–8 PF_6^- counterions and, hence, having 1–8 positive charges, which showed the theoretically expected isotope patterns. For **G1Ru4Fe1**, six intense ESI MS peaks were observed (Fig. S2a, ESI†) at

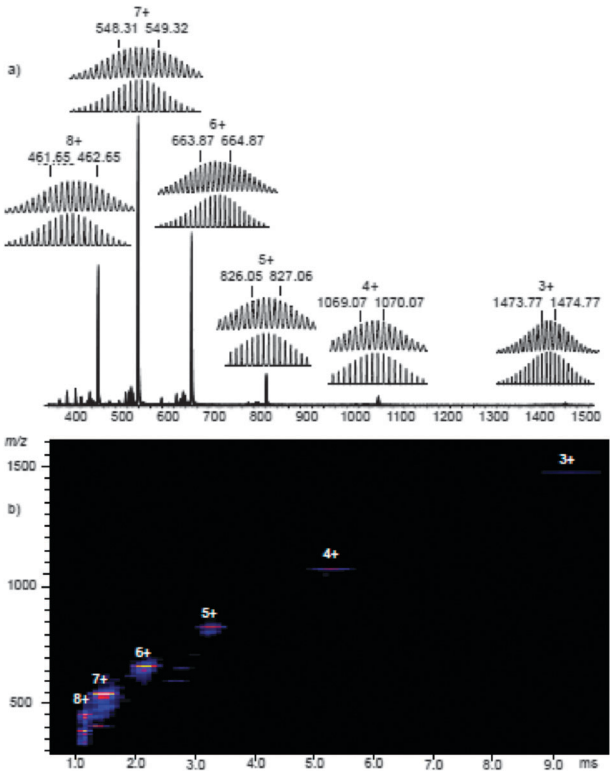

Fig. 4 (a) ESI MS of **G1Ru5**. (b) Two-dimensional ESI-TWIM MS plot (m/z *vs.* drift time) of **G1Ru5**, acquired using a traveling wave velocity of 350 m s^{-1} and a traveling wave height of 8.5 V.

m/z 1459.1 $[M - 3PF_6]^{3+}$ (calcd m/z = 1459.1), 1057.8 $[M - 4PF_6]^{4+}$ (calcd m/z = 1058.1), 817.4 $[M - 5PF_6]^{5+}$ (calcd m/z = 817.5), 657.0 $[M - 6PF_6]^{6+}$ (calcd m/z = 657.1), 542.5 $[M - 7PF_6]^{7+}$ (calcd m/z = 542.5), and 456.5 $[M - 8PF_{6-}]^{8+}$ (calcd m/z = 456.6) with the correct isotope patterns. Meanwhile, ESI MS of **G0** and **G1Ru5** generated a continuous series of peaks with +2 to +6 charges and +3 to +8 charges, respectively, which showed isotope distributions that are in accord with the corresponding calculated distributions (Fig. 4, Fig. S1, and S2, ESI†). In order to resolve any superimposed fragments and determine whether overlapping isomers of the complexes exist, ESI-TWIM MS was used as a second level of MS analysis, for separation based on differences in ion mobilities. In mobility experiments, ions are dispersed not only on the basis of their m/z ratios but also according to their molecular sizes and shapes. In all cases (Fig. 4, Fig. S1, and S2, ESI†), the desired compounds are the predominant species; a few minor fragments are observed, but the presence of isomers or byproducts is excluded. The drift times of the charge states formed by the Ru(II)/Fe(II) dendrimers can be obtained from the two dimensional ESI-TWIM MS plots. Compact and smaller ions drift faster, while more extended and larger ions drift more slowly.[12,13] For example, the ESI-TWIM MS plot in Fig. 4 reveals that the $[M - 3PF_6]^{3+}$, $[M - 4PF_6]^{4+}$, $[M - 5PF_6]^{5+}$, $[M - 6PF_6]^{6+}$, and $[M - 7PF_6]^{7+}$ ions from **G1Ru5** have drift times of 9.21, 5.14, 3.16, 1.99, and 1.35 ms, respectively; whereas the +2 to +5 charge states of **G0** have drift times at 9.21, 3.70, 1.99, and 1.08 ms (see ESI†). The drift times of the same charge states dramatically increased from **G0** to **G1Ru5**, which is consistent with the concomitant increase in the corresponding dendrimer sizes. Moreover, **G1Ru5** and **G1Ru4Fe1** have similar drift times in charge states +3 to +7 due to their identical backbones, in spite of the different metal ion cores. Such results indicate that drift time data can provide valuable information about the differences or similarities between unique supramolecular architectures.

To examine the relative stabilities of the metallodendrimers with different metal ion cores, gradient tandem MS (gMS^2) experiments were performed on charge state +4 from both **G1Ru4Fe1** (m/z = 1058) as well as **G1Ru5** (m/z = 1069), which were subjected to collision-activated dissociation (CAD) with Ar before ion mobility separation at collision energies ranging from 6 to 65 eV (Fig. S2 and S3, ESI†). After initially losing neutral PF_5 units, these complexes dissociate further, disappearing completely when the trap voltage reaches 45 V for **G1Ru4Fe1** and 65 V for **G1Ru5**. From these results, the center-of-mass collision energy (E_{cm}) of disappearance can be calculated as 1.69 eV for **G1Ru4Fe1** and 2.41 eV for **G1Ru5**, which gives direct evidence for the lower stability of the ⟨tpy-Fe^{II}-tpy⟩ connecter under ESI MS^2 conditions.

As mentioned in the Introduction, single crystals afford direct evidence for structural identification. Single crystals of both the initial ligand **MT3** and complex **G0** were realized. The single crystal of ligand **MT3** was grown from a saturated $CHCl_3$ solution (Fig. 5a). The structure revealed distortions among the pyridine rings of the mesitylene–terpyridines, which result from the free rotation around the bonds; however, the steric interactions between the 3′,5′ protons on the terpyridine moieties and the protons on the methyl groups restrict rotation about the terpyridine–mesitylene carbon–carbon connective bond.[18]

A single crystal of the complex **G0** was obtained from a MeOH solution. Each of the central pyridine rings for the mesitylene terpyridines was found to be nearly perpendicular (82.7°) to the focal mesitylene, while the terminal terpyridine

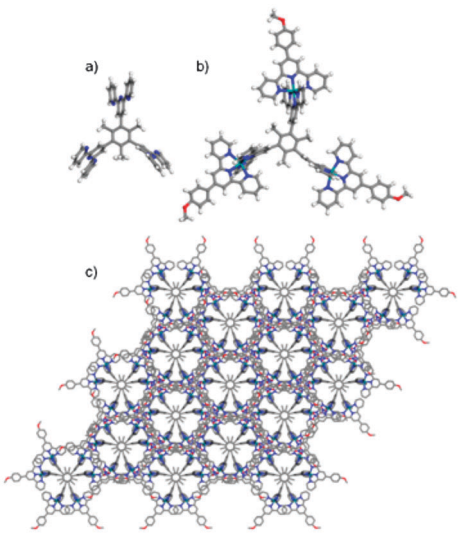

Fig. 5 (a) Single crystal X-ray structure of ligand **MT3**; (b) X-ray single crystal of the network building block **G0** viewed from the *c*-axis; (c) honey-comb-like packing pattern of the crystalline network of complex **G0** viewed from the *c*-axis (see ESI† part 5 for pertinent X-ray data for **G0** and **MT3**).

moieties were observed to be almost parallel to the mesitylene moiety (Fig. 5b). This is most likely a result of a slight distortion from the idealized octahedral geometry between the binding terpyridines and Ru(II) center (the angle of the ⟨N–Ru–N⟩ band is about 176.5°).

The outer distances between the methyl groups on the capping terpyridines were observed to be 31.8 Å, forming an equilateral triangle around the perimeter of the molecule. The Ru–Ru distance for each of the three units was 12.99 Å. The resultant molecular packing revealed a unique honeycomb-like pattern (Fig. 5c), which arises as a result of the stacking of the central mesitylene rings, as well as a direct overlap between the 4,6 and 4′′,6′′ carbons in the terpyridine moiety. The interplanar distance between the stacked mesitylene rings was calculated to be 10.8 Å. The substituents on the central ring are arranged in a gauche-like conformation with an angle of 29.1° between the methyl groups and 34.0° between the terpyridine rings (when viewed along the *c*-axis). Notably, the internal methyl groups also restrict rotation, as in **MT3** and the molecule lies on a 3-fold axis. A Flack value of 0.32(6) indicates an inversion twin.

The absorption and emission spectra of the metallodendrimers in dilute MeOH and the corresponding tris-ligand **MT3** in dilute $CHCl_3$ are shown in Fig. 6 and summarized in Table 1. Ligand **MT3** exhibits a ligand-centered, $\pi \rightarrow \pi^*$ transition (LC) at *ca.* 280 nm. Compared with the ligand, the Ru(II) or Ru/Fe(II) complexes exhibited two distinct absorption bands. The one possessing a shorter wavelength belongs to the absorption of the tris-terpyridine ligands (**T3** or **MT3**) at about 282–293 nm and mono-capping ligand **3** at *ca.* 307 nm; the latter peak became more distinct upon increasing the relative content of ligand **3** in the complexes compared with tris-ligands. The other absorptions for the Ru(II) complexes at longer wavelengths were centered at 490–497 nm, which is attributed to the metal-to-ligand charge

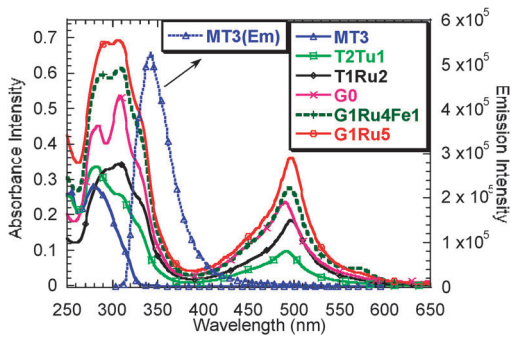

Fig. 6 Absorption and emission spectra of ligand **MT3** and the complexes, acquired in dilute MeOH (2.5×10^{-6} M) at 25 °C. The excitation wavelength in the emission experiments of ligand **MT3** was 280 nm.

Table 1 Photophysical properties of the complexes and ligand **TM3** in dilute MeOH (2.5×10^{-6} M) at 25 °C

Compounds	λ_{max} abs./nm ($\varepsilon \times 10^{-5}$)	λ_{max} emis./nm
TM3	280 (1.05)	340
T2Ru1	282 (1.32), 492 (0.38)	
T1Ru2	308 (1.36), 497 (0.73)	
G0	284 (1.80), 308 (2.14), 490 (0.96)	
G1Ru5	293 (2.75), 307 (2.76), 497 (1.44)	
G1Ru4Fe1	286 (2.40), 324 (2.48), 495 (1.12), 568 (0.2)	

transfer (MLCT) transition of ⟨tpy-Ru^{II}-tpy⟩ chromophores. Moreover, a slight blue shift is observed for **G0** due to the steric hindrance of the methyl group. Heterocomplexes **G1Ru4Fe1** give rise to a similar band at 495 nm plus the MLCT band of the ⟨tpy-Fe^{II}-tpy⟩ chromophore at 568 nm. Molar extinction coefficients progressively increase from ligand **MT3** to metallodendrimer **G0** to **G1Ru5**, as expected from the increasing number of ligand chromophores and metal ion centers. The broad and strong absorption of three metallodendrimers is beneficial to the light-harvesting process. Only the ligand is fluorescent in dilute solution and the emission maximum in $CHCl_3$ peaks at 340 nm. Meanwhile, all Ru(II) or Ru/Fe(II)-complexes are non-emissive, as a result of the fast relaxation of the Ru/Fe(II)-terpyridine complex to the ground state.[19]

The electrochemical properties of these complexes and ligand **MT3** were investigated by cyclic voltammetry in DMF and $Ag/AgNO_3$, as reference electrode. Relevant electrochemical data are listed in Table 2 and Fig. 7. The ligand **MT3** showed only one reversible reduction process that peaked at *ca.* −2.35 V; whereas, the corresponding complexes showed two quasi-reversible one-electron reduction processes at about −1.7 V and −1.9 V *vs.* $Ag/AgNO_3$ that can be assigned to a sequential one-electron reduction of the two terpyridine ligands surrounding the complexed Ru/Fe(II) metal ions (tpy/tpy^- and tpy^-/tpy^{2-}). Inspection of the cathodic region revealed that a third irreversible reduction peak followed the two-wave reduction process that is related to a further reduction at the coordinated terpyridine units. Interestingly for **T1Ru2** and **T2Ru1**, there is a fourth cathodic peak whose intensity decreased from **T2Ru1** to **T1Ru2**. These results suggested that the electron was from the uncoordinated terminal terpyridine groups, which is consistent with ligand **MT3**. All complexes exhibit one quasi-reversible oxidation wave due to the Ru^{III}/Ru^{II} or Fe^{III}/Fe^{II} couples. From the measured $E_{ox(onset)}$ values, the energies of the corresponding highest occupied molecular orbital (HOMO) can be calculated according to eqn (1).

$$E_{HOMO} = -e(E_{ox(onset)} + 4.71)\ (eV) \quad (1)$$

Table 2 Electrochemical peaks, onset potentials and energy levels of metallodendrimers and ligand[a]

Compound	$E_{ox(peak)}$/V	$E_{ox(onset)}$/V	$E_{red(peak)}$/V	$E_{red(onset)}$/V	E_{HOMO}/eV	E_{LUMO}/eV	$E_{g(cv)}$/eV	$E_{g(opt)}$/eV
MT3	—	—	−2.42/−2.60	−2.35	−6.11	−2.36	—	3.75
T2Ru1	0.82	0.68	−1.67, −1.92, −2.32, −2.44	−1.55	−5.39	−3.16	2.23	2.17
T1Ru2	0.83	0.71	−1.65, −1.92, −2.37, −2.52	−1.55	−5.42	−3.16	2.26	2.18
G0	0.85	0.69	−1.67, −1.93, −2.42	−1.55	−5.40	−3.16	2.24	2.19
G1Ru5	0.85	0.72	−1.64, −1.92, −2.38	−1.52	−5.43	−3.19	2.24	2.17
G1Ru4Fe1	0.84	0.68	−1.68, −1.93, −2.37	−1.46	−5.39	−3.25	2.14	2.08

[a] Scan rate: 100 mV s^{-1}; working electrode: Pt disc; auxiliary electrode: Pt wire; reference electrode: $Ag/AgNO_3$; supporting electrolyte: Bu_4NPF_6 (0.1 M, DMF).

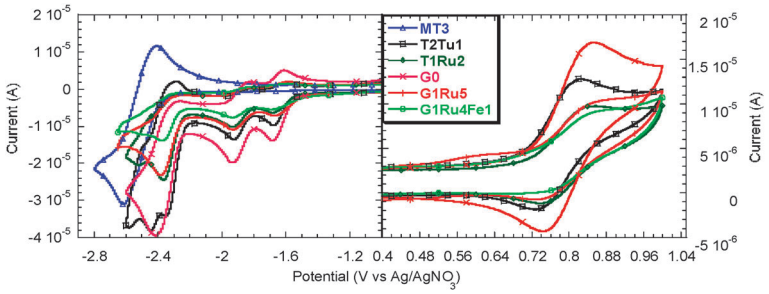

Fig. 7 Cyclic voltammogram of metallodendrimers and ligand in a 0.1 M solution of Bu_4NPF_6 in DMF, acquired at a scan rate of 100 mV s^{-1}. For both scans shown, the bottom traces (reduction) were scanned from right to left and the upper traces (oxidation) were scanned from left to right.

$E_{ox(onset)}$ is the onset of oxidation potential *vs.* $Ag/AgNO_3$.[20] Similarly, the energy of the lowest unoccupied molecular orbital can be estimated from the value of $E_{red(onset)}$ *via* eqn (2).

$$E_{LUMO} = -e(E_{red(onset)} + 4.71)\ (eV) \qquad (2)$$

The electrochemical band gaps $E_{g(cv)}$, calculated by subtracting the HOMO from the LUMO energy, albeit slightly larger, are consistent with the corresponding optical band gaps, $E_{g(opt)}$, which corresponds well with the work of Bäurele *et al.*[21] Notably, electrostatic interactions in solution that result from a wide range of oxidation state variations are under consideration.

Conclusions

A family of well-defined shape-persistent and small, rigid metallodendrimers **G0**, **G1Ru5**, and **G1Ru4Fe1**, based on ⟨tpy-Ru^{II}-tpy⟩ or ⟨tpy-Fe^{II}-tpy⟩ connectivity as either the branch or core center has been prepared from two simple ligands *via* a self-assembly approach. The resulting products were purified by column chromatography and their molecular structures as well as sizes were elucidated by NMR and ESI-TWIM MS, and single crystal X-ray data. Introduction of higher generation dendritic structures and multiple metal ion centers results in higher molar extinction coefficients in a broad absorption region. The photo-physical and electrochemical properties of these complexes exhibited noticeable changes that are quantitatively expected based on the number of electro-active moieties within dendron generation. These materials provide interesting platforms for fine-tuning spin crossover applications as well as for sensitizer components of solar cells.

Experimental section

General procedures

Chemicals were commercially purchased and used without further purification. Thin layer chromatography (TLC) was conducted on flexible sheets (Baker-flex) precoated with Al_2O_3 (IB-F) or SiO_2 (IB2-F) and the separated products were visualized by UV light. Column chromatography was conducted using basic Al_2O_3, Brockman Activity I (60–325 mesh) or SiO_2 (60–200 mesh) from Fisher Scientific. ^1H and ^{13}C NMR spectra were recorded on a Varian NMRS 500 spectrometer using $CDCl_3$, except where noted. UV-vis spectra were recorded on a Perkin Elmer Lambda 35 UV-vis spectrometer. PL spectra were conducted on a Perkin Elmer LS55 luminescence spectrometer. Cyclic voltammetry was performed using a BASi EC epsilon workstation; scan rate: 100 mV s^{-1}; working electrode: Pt disc; auxiliary electrode: Pt wire; reference electrode: $Ag/AgNO_3$ ($Ag/AgNO_3$ chosen for comparison,[11] notably, decamethylferrocene may prove more useful); supporting electrolyte: Bu_4NPF_6 (0.1 M, DMF). ESI mass spectra were obtained on a Bruker Esquire quadrupole ion trap mass spectrometer (ESI MS) or a Waters Synapt HDMS quadrupole/time-of-flight (Q/ToF) tandem mass spectrometer. MALDI-ToF MS measurements were performed with a Bruker UltraFlex III ToF/ToF mass spectrometer, equipped with a Nd:YAG laser emitting at a wavelength of 355 nm. The TWIM MS experiments were performed on the Synapt mass spectrometer using the following parameters: ESI capillary voltage: 1.0 kV; sample cone voltage: 7 V; extraction cone voltage: 3.2 V; desolvation gas flow: 800 L h^{-1} (N_2); trap collision energy (CE): 1 eV; transfer CE: 1 eV; trap gas flow: 1.5 mL min^{-1} (Ar); ion mobility cell gas flow: 22.7 mL min^{-1} (N_2); sample flow rate: 5 μL min^{-1}; source temperature: 30 °C; desolvation temperature: 40 °C; IM travelling wave height: 8.5 V; and IM travelling wave velocity: 350 m s^{-1}. The sprayed solution was prepared by dissolving ~0.3 mg of sample in 1 mL of a MeCN/MeOH (1 : 1, v/v) mixture. Data analyses were conducted using the MassLynx 4.1 and DriftScope 2.1 programs provided by Waters.

Syntheses

Tris-terpyridines—T3 and **MT3**. To 1,3,5-triformylbenzene (600 mg, 3.7 mmol), 2-acetylpyridine (3.02 g, 24.4 mmol) and NaOH (1.21 g, 29.6 mmol) were added and ground using a mortar and pestle; the yellow medium was aggregated until a yellow solid resulted. The solid was transferred to a 250 mL flask and EtOH (80 mL) was added. After stirring at 25 °C for 2 h, aqueous NH_4OH (80 mL, 28–30%) was added. The mixture was refluxed for 20 h, then the precipitate was filtered and the solid was purified by column chromatography (Al_2O_3) eluting with $CHCl_3$ to give **T3**, as a white solid: 880 mg (31%); mp 316–318 °C; ^1H NMR (500 MHz): δ 8.89 (s, 6H, Py-$H^{3',5'}$), 8.73–8.74 (d, J = 4.5 Hz, 6H, Py-$H^{6,6''}$), 8.70–8.72 (d, J = 8.0 Hz, 6H, Py-$H^{3,3''}$), 8.42 (s, 3H, Ph-*H*), 7.89–7.92 (dt, 6H, J = 8.0, 1.5 Hz, Py-$H^{4,4''}$), 7.36–7.38 (m, 6H, Py-$H^{5,5''}$); ^{13}C NMR (125 MHz): δ 156.32, 156.29, 150.1, 149.4, 140.8, 137.1, 121.3, 124.1, 121.6, 119.7; MALDI-ToF MS (*m*/*z*): calcd for $C_{51}H_{33}N_9$: 771.3. Found: 772.3 ($[M + H]^+$).

To 1,3,5-triformyl-2,4,6-trimethylbenzene (1.50 g, 7.35 mmol), 2-acetylpyridine (5.87 g, 48.4 mmol) and NaOH (2.35 g, 58.8 mmol)

were added and then ground using a mortar and pestle. The yellow medium was aggregated until a yellow solid was formed. The solid was transferred to a 500 mL flask and was dissolved in EtOH (150 mL). After stirring at 25 °C for 2 h, aqueous NH_4OH (160 mL, 28–30%) was added into the mixture. After refluxing for 20 h, the precipitate was filtered, purified by column chromatography (Al_2O_3) using $CHCl_3$, as eluent, to give **MT3**, as a white solid: 1.50 g (25%); mp 378–380 °C; ^{1}H NMR (500 MHz): δ 8.75–8.76 (d, J = 4.0 Hz, 6H, Py-$H^{6,6''}$), 8.71–8.72 (d, J = 8.0 Hz, 6H, Py-$H^{3,3''}$), 8.43 (s, 6H, Py-$H^{3',5'}$), 7.89–7.92 (m, 6H, Py-$H^{4,4''}$), 7.35–7.37 (m, 6H, Py-$H^{5,5''}$), 1.96 (s, 9H, CH_3); ^{13}C NMR (125 MHz): δ 156.3,156.0, 152.3, 149.4, 138.4, 136.9, 132.4, 123.9, 122.3, 121.3, 19.8; MALDI-ToF MS (m/z): calcd for $C_{54}H_{39}N_9$: 813.3. Found: 814.4 ($[M + H]^+$).

Mono- and bis-metallated tris-terpyridines—T2Ru1 and **T1Ru2**. Tris-ligand **T3** (154.4 mg, 200 μmol) was added to a suspension of mono(Ru^{III}) adduct **4** (218.4 mg, 400 μmol) in MeOH and $CHCl_3$ (75 mL, 2 : 1), then *N*-ethylmorpholine (4 drops) was added. The mixture was refluxed for additional 15 h. The red solution was filtered through Celite, then the filtrate was concentrated *in vacuo* to give a residue, which was flash column chromatographed (Al_2O_3) using H_2O/MeCN/sat.KNO_3(aq.), as the mobile phase to successively elute **T2Ru1** (solvent composition, 1/20/1, v/v/v), and **T1Ru2** (solvent composition, 1/15/1, v/v/v), which were isolated as red solids.

Data for T2Ru1. 54 mg (18%); ^{1}H NMR (CD_3OD/$CDCl_3$, 3/1, 500 MHz): δ 9.52 (s, 2H, ^{b}Py-$H^{3',5'}$), 9.17 (s, 6H, ^{a}Py-$H^{3',5'}$), 9.03–9.06 (m, 6H, ^{b}Py-$H^{3,3''}$, ^{c}Py-$H^{3',5'}$), 8.98 (d, J = 1.0 Hz, 2H, Ph-$H^{x,y}$), 8.83–8.84 (d, 2H, J = 8.0 Hz, ^{a}Py-$H^{3,3''}$), 8.73–8.75 (m, 9H, ^{c}Py-$H^{3,3''}$, ^{c}Py-$H^{6,6''}$, Ph-H^z), 8.20–8.22 (d, J = 9.0 Hz, 2H, Ph-H), 8.01–8.06 (m, 8H, ^{a,b,c}Py-$H^{4,4''}$), 7.50–7.54 (m, 8H, ^{a,b}Py-$H^{6,6''}$, ^{c}Py-$H^{5,5''}$), 7.30–7.32 (m, 4H, ^{a,b}Py-$H^{5,5''}$), 7.25–7.27 (d, J = 9.0 Hz, 2H, Ph-H), 3.98 (s, 3H, OCH_3); ^{13}C NMR (CD_3OD/$CDCl_3$, 3/1, 125 MHz): δ 163.2, 159.4, 159.2, 157.4, 156.9, 156.8, 156.2, 153.0, 152.9, 150.2, 150.05, 150.00, 148.5, 141.7, 139.6, 139.5, 139.3, 138.6, 130.1, 129.6, 128.9, 128.8, 128.4, 128.3, 126.1, 125.9, 125.4, 123.0, 122.5, 121.8, 120.2, 116.1, 56.2; MALDI-ToF MS (m/z): calcd for $C_{73}H_{50}F_{12}N_{12}OP_2Ru$: 1502.3. Found: 1357.5 $(M - PF_6^-)^+$, 1212.5 $(M + H^+ - 2PF_6^-)^+$.

Data for T1Ru2. 210 mg (48%); ^{1}H NMR (CD_3OD/$CDCl_3$, 3/1, 500 MHz): δ 9.66 (s, 4H, ^{b}Py-$H^{3',5'}$), 9.42 (s, 1H, Ph-H^y), 9.20 (m, 6H, ^{a}Py-$H^{3',5'}$, Ph-$H^{x,z}$), 9.11–9.13 (d, 4H, J = 8.0 Hz, ^{b}Py-$H^{3,3''}$), 9.10 (s, 2H, ^{c}Py-$H^{3',5'}$), 8.85–8.87 (d, 4H, J = 8.0 Hz, ^{a}Py-$H^{3,3''}$), 8.81–8.85 (m, 4H, ^{c}Py-$H^{3,3''}$, ^{c}Py-$H^{6,6''}$), 8.24–8.26 (d, J = 8.5 Hz, 2H, Ph-H), 8.09–8.11 (m, 2H, ^{c}Py-$H^{4,4''}$), 8.01–8.08 (m, 10H, ^{a,b}Py-$H^{4,4'}$), 7.64–7.65 (d, 4H, J = 5.5 Hz, ^{b}Py-$H^{6,6''}$), 7.55–7.59 (m, 6H, ^{a}Py-$H^{6,6''}$, ^{c}Py-$H^{5,5''}$), 7.31–7.35 (m, 8H, ^{a,b}Py-$H^{5,5''}$), 7.27–7.29 (d, J = 8.5 Hz, 4H, Ph-H), 3.99 (s, 6H, OCH_3); ^{13}C NMR (CD_3OD/$CDCl_3$, 3/1, 125 MHz): δ 163.3, 159.7, 159.6, 157.6, 157.2, 157.1, 156.5, 153.4, 153.1, 150.5, 150.2, 150.1, 148.9, 142.2, 140.8, 139.5, 139.4, 139.2, 130.3, 129.9, 129.7, 129.1, 129.02, 129.00, 126.5, 125.9, 125.8, 123.41, 123.38, 121.93, 120.3, 116.2, 56.2; MALDI-ToF MS (m/z): calcd for $C_{95}H_{67}F_{24}N_{15}O_2P_2Ru_2$: 2233.2. Found: 2087.4 $(M - PF_6^-)^+$, 1940.4 $(M + H^+ - 2PF_6^-)^+$.

Tris-metallated tris-terpyridine—G0. Tris-terpyridine ligand **MT3** (40.6 mg, 50 μmol) was added to a suspension of mono(Ru^{III}) adduct **4** (97.0 mg, 180 μmol) in MeOH and $CHCl_3$ (45 mL, 2 : 1), then *N*-ethylmorpholine (4 drops) was added. The mixture was refluxed for additional 15 h. The red solution was filtered through Celite and concentrated *in vacuo* to give a residue, which was flash column chromatographed (silica gel) eluting with (H_2O/MeCN/sat. KNO_3(aq), 1/12/1) to afford the product with salt. After washing with water, the red solid was dissolved in MeOH, and was concentrated as a red solid: 65 mg (52%); ^{1}H NMR (CD_3OD/$CDCl_3$, 3/1, 500 MHz): δ 9.21 (s, 6H, ^{a}Py-$H^{3',5'}$), 9.14 (s, 6H, ^{b}Py-$H^{3',5'}$), 8.89–8.91 (d, 6H, J = 8.0 Hz, ^{a}Py-$H^{3,3''}$), 8.82–8.84 (d, 6H, J = 8.0 Hz, ^{b}Py-$H^{3,3''}$), 8.20–8.22 (d, J = 8.5 Hz, 6H, Ph-H), 7.98–8.03 (m, 12H, ^{a,b}Py-$H^{4,4''}$), 7.50–7.53 (m, 12H, ^{a,b}Py-$H^{6,6''}$), 7.33–7.36 (m, 6H, ^{a}Py-$H^{5,5''}$), 7.29–7.31 (m, 6H, ^{b}Py-$H^{5,5''}$), 7.22–7.24 (d, J = 8.5 Hz, 6H, Ph-H), 3.96 (s, 9H, OCH_3). 2.57 (s, 9H, CH_3); ^{13}C NMR (CD_3CN, 125 MHz): δ 162.9, 159.2, 156.8, 156.2, 152.9, 152.8, 150.9, 149.9, 139.3, 138.2, 135.5, 130.0, 129.5, 129.0, 128.9, 126.5, 126.3, 125.8, 121.7, 115.9, 56.1, 20.9; MALDI-ToF MS (m/z): calcd for $C_{120}H_{90}F_{36}N_{18}O_3P_3Ru_3$: 3006.2. Found: 2860.8 $(M - PF_6^-)^+$, 1358.4 $(M - 2PF_6^-)^{2+}$; ESI MS (m/z): 1358.3 $[M - 2PF_6^-]^{2+}$ (calcd m/z = 1358.2), 857.2 $[M - 3PF_6^-]^{3+}$ (calcd m/z = 857.1), 606.6 $[M - 4PF_6^-]^{4+}$ (calcd m/z = 606.6), 456.1 $[M - 5PF_6^-]^{5+}$ (calcd m/z = 456.3), 355.9 $[M - 6PF_6^-]^{6+}$ (calcd m/z = 356.1).

Homo- and heterogenous multinuclear dendritic materials—G1Ru5. Solid $RuCl_2(DMSO)_4$ (12.2 mg, 25.2 mmol) was added to a stirred solution of **T1Ru2** (95.1 mg, 50 μmol) in MeOH (100 mL). After the mixture refluxing for 10 h, the red solution was concentrated *in vacuo* to give a residue, which was purified by flash column chromatography (SiO_2) using a H_2O/MeCN/sat. KNO_3(aq.) (1/8/1 v/v/v) mixture, as eluent, to afford the red solid: 71 mg (70%); ^{1}H NMR (CD_3OD/$CDCl_3$, 3/1, 500 MHz): δ 9.80 (s, 4H, ^{c}Py-$H^{3',5'}$), δ 9.77 (s, 8H, ^{b}Py-$H^{3',5'}$), 9.45–9.46 (m, 6H, Ph-$H^{x,y,z}$), 9.18 (s, 8H, ^{a}Py-$H^{3',5'}$), 9.15–9.16 (d, 4H, J = 8.0 Hz, ^{c}Py-$H^{3,3''}$), 9.11–9.13 (d, 8H, J = 8.0 Hz, ^{b}Py-$H^{3,3''}$), 8.83–8.85 (d, 8H, J = 8.0 Hz, ^{a}Py-$H^{3,3''}$), 8.22–8.24 (d, J = 8.5 Hz, 8H, Ph-H), 8.00–8.08 (m, 20H, ^{a,b,c}Py-$H^{4,4''}$), 7.74–7.75 (d, 4H, J = 5.5 Hz, ^{c}Py-$H^{6,6''}$), 7.69–7.70 (d, 8H, J = 5.5 Hz, ^{b}Py-$H^{6,6''}$), 7.53–7.54 (d, 8H, J = 5.5 Hz, ^{a}Py-$H^{6,6''}$), 7.38–7.41 (m, 4H, ^{c}Py-$H^{5,5''}$), 7.34–7.37 (m, 8H, ^{b}Py-$H^{5,5''}$), 7.27–7.30 (m, 8H, ^{a}Py-$H^{5,5''}$), 7.26–7.27 (d, J = 8.5 Hz, 8H, Ph-H), 3.99 (s, 12H, OCH_3); ^{13}C NMR (CD_3OD/$CDCl_3$, 3/1, 125 MHz): δ 163.1, 159.6, 159.5, 159.3, 156.92, 156.90, 156.4, 153.5, 153.2, 152.7, 150.0, 148.9, 148.8, 140.9, 140.8, 139.5, 139.3, 130.1, 129.6, 128.9, 128.8, 126.5, 125.7, 123.7, 123.6, 121.7, 116.0, 56.1; MALDI-ToF MS (m/z): calcd for $C_{190}H_{134}F_{60}N_{30}O_4P_{10}Ru_5$: 4858.3. Found: 4712.7 $(M - PF_6^-)^+$, 2283.8 $(M - 2PF_6^-)^{2+}$; ESI MS (m/z): 1474.1 $[M - 3PF_6^-]^{3+}$ (calcd m/z = 1474.1), 1069.3 $[M - 4PF_6^-]^{4+}$ (calcd m/z = 1069.4), 826.5 $[M - 5PF_6^-]^{5+}$ (calcd m/z = 826.5), 664.5 $[M - 6PF_6^-]^{6+}$ (calcd m/z = 664.6), 548.9 $[M - 7PF_6^-]^{7+}$ (calcd m/z = 548.9), 462.2 $[M - 8PF_6^-]^{8+}$ (calcd m/z = 462.2), 394.7 $[M - 9PF_6^-]^{9+}$ (calcd m/z = 394.7), and 340.8 $[M - 10PF_6^-]^{10+}$ (calcd m/z = 340.8).

G1Ru4Fe1. A solution of $FeCl_2{\cdot}4H_2O$ (50.0 mg, 25.1 μmol) in MeOH (100 mL) was added to a stirred solution of **T1Ru2** (95.1 mg, 50 μmol) in MeOH (100 mL). After stirring the mixture at 25 °C for 10 h, the purple solution was concentrated *in vacuo* to give a residue, which was purified by flash column chromatography (SiO_2) using a H_2O/MeCN/sat. KNO_3(aq.) (1/7/1 v/v/v) mixture as eluent to afford the dark solid: 84 mg (84%); ^{1}H NMR ($CD_3OD/CDCl_3$, 3/1, 500 MHz): δ 9.97 (s, 4H, ^{c}Py-$H^{3',5'}$), δ 9.79 (s, 8H, ^{b}Py-$H^{3',5'}$), 9.57 (s, 4H, Ph-$H^{x,z}$), 9.50 (s, 2H, Ph-H^{y}), 9.15 (s, 8H, ^{a}Py-$H^{3',5'}$), 9.12–9.14 (d, 8H, J = 8.0 Hz, ^{b}Py-$H^{3,3''}$), 9.09–9.11 (d, 4H, J = 8.0 Hz, ^{c}Py-$H^{3,3''}$), 8.81–8.83 (d, 8H, J = 8.0 Hz, ^{a}Py-$H^{3,3''}$), 8.19–8.21 (d, J = 8.5 Hz, 8H, Ph-*H*), 8.00–8.06 (m, 20H, ^{a,b,c}Py-$H^{4,4''}$), 7.68–7.70 (d, 4H, J = 5.5 Hz, ^{b}Py-$H^{6,6''}$), 7.48–7.50 (m, 12H, ^{a,c}Py-$H^{6,6''}$), 7.35–7.37 (m, 8H, ^{b}Py-$H^{5,5''}$), 7.29–7.31 (m, 12H, ^{a,c}Py-$H^{5,5''}$), 7.25–7.26 (d, J = 8.5 Hz, 8H, Ph-*H*), 3.98 (s, 12H, OCH_3); ^{13}C NMR ($CD_3OD/CDCl_3$, 3/1, 125 MHz): δ 163.1, 161.9, 159.7, 159.41, 159.38, 157.0, 156.4, 153.9, 153.5, 152.8, 151.0, 150.0, 148.8, 141.0, 140.8, 140.1, 139.5, 139.3, 130.4, 130.2, 130.1, 129.7, 129.0, 128.8, 126.5, 125.8, 123.7, 123.5, 121.8, 116.0, 56.1; ESI MS (m/z): 1459.1 $[M - 3PF_6^-]^{3+}$ (calcd m/z = 1459.1), 1058.1 $[M - 4PF_6^-]^{4+}$ (calcd m/z = 1058.1), 817.4 $[M - 5PF_6^-]^{5+}$ (calcd m/z = 817.5), 657.0 $[M - 6PF_6^-]^{6+}$ (calcd m/z = 657.1), 542.5 $[M - 7PF_6^-]^{7+}$ (calcd m/z = 542.5), 456.5 $[M - 8PF_6^-]^{8+}$ (calcd m/z = 456.6).

Acknowledgements

The authors gratefully thank the National Science Foundation (DMR-0812337 and DMR-0705015 to GRN; CHE-1012636 and DMR-0821313 to CW) and the Ohio Board of Regents for financial support.

Notes and references

1 (*a*) J.-M. Lehn, *Supramolecular Chemistry: Concepts and Perspectives*, VCH, Weinheim, 1995; (*b*) D. Philip and J. F. Stoddart, *Angew. Chem., Int. Ed. Engl.*, 1996, **35**, 1155–1196; (*c*) S. Leininger, B. Olenyuk and P. J. Stang, *Chem. Rev.*, 2000, **100**, 853–908; (*d*) B. J. Holliday and C. A. Mirkin, *Angew. Chem., Int. Ed.*, 2001, **40**, 2022–2043; (*e*) G. M. Whitesides and B. Grzybowski, *Science*, 2002, **295**, 2418–2421; (*f*) B. H. Northrop, Y. R. Zheng, K. W. Chi and P. J. Stang, *Acc. Chem. Res.*, 2009, **42**, 1554–1563.

2 (*a*) M. Fujita, J. Yazaki and K. Ogura, *J. Am. Chem. Soc.*, 1990, **112**, 5645–5647; (*b*) T. Bark, M. Düggeli, H. Stoeckli-Evans and A. von Zelewsky, *Angew. Chem., Int. Ed.*, 2001, **40**, 2848–2851; (*c*) T. Megyes, H. Jude, T. Grosz, I. Bako, T. Radnai, G. Tarkanyi, G. Palinkas and P. J. Stang, *J. Am. Chem. Soc.*, 2005, **127**, 10731–10738; (*d*) K. Mahata, M. L. Saha and M. Schmittel, *J. Am. Chem. Soc.*, 2010, **132**, 15933–15935; (*e*) Y.-T. Chan, C. N. Moorefield, M. Soler and G. R. Newkome, *Chem.–Eur. J.*, 2010, **16**, 1768–1771; (*f*) J.-L. Wang, X. Li, X. Lu, I.-F. Hsieh, Y. Cao, C. N. Moorefield, C. Wesdemiotis, S. Z. D. Cheng and G. R. Newkome, *J. Am. Chem. Soc.*, 2011, **133**, 11450–11453.

3 (*a*) M. Fujita, M. Tominaga, A. Hori and B. Therrien, *Acc. Chem. Res.*, 2005, **38**, 369–378; (*b*) M. Yoshizawa, J. K. Klosterman and M. Fujita, *Angew. Chem., Int. Ed.*, 2009, **48**, 3418–3438; (*c*) K. Ghosh, J. Hu, H. S. White and P. J. Stang, *J. Am. Chem. Soc.*, 2009, **131**, 6695–6697; (*d*) Q. F. Sun, J. Iwasa, D. Ogawa, Y. Ishido, S. Sato, T. Ozeki, Y. Sei, K. Yamaguchi and M. Fujita, *Science*, 2010, **328**, 1144–1147.

4 (*a*) C. G. Oliveri, P. A. Ulmann, M. J. Wiester and C. A. Mirkin, *Acc. Chem. Res.*, 2008, **41**, 1618–1629; (*b*) Y.-R. Zheng, Z. Zhao, M. Wang, K. Ghosh, J. B. Pollock, T. R. Cock and P. J. Stang, *J. Am. Chem. Soc.*, 2010, **132**, 16873–16882.

5 (*a*) D. Armspach, M. Cattalini, E. C. Constable, C. E. Housecroft and D. Phillips, *Chem. Commun.*, 1996, 1823–1824; (*b*) S. Serroni, S. Campagna, F. Puntoriero, C. Di Pietro, N. D. McClenaghan and F. Loiseau, *Chem. Soc. Rev.*, 2001, **30**, 367–375.

6 (*a*) A. Adronov and J. M. J. Fréchet, *Chem. Commun.*, 2000, 1701–1710; (*b*) R. M. Crooks, M. Zhao, L. Sun, V. Chechik and L. K. Yeung, *Acc. Chem. Res.*, 2001, **34**, 181–190; (*c*) J. Pei, J.-L. Wang, X.-Y. Cao, X.-H. Zhou and W.-B. Zhang, *J. Am. Chem. Soc.*, 2003, **125**, 9944–9945; (*d*) W.-S. Li, D.-L. Jiang, Y. Suna and T. Aida, *J. Am. Chem. Soc.*, 2005, **127**, 7700–7702; (*e*) G. R. Newkome and C. D. Shreiner, *"Designer Monomers to Tailored Dendrimers"*, in *Synthesis of Designer Dendrimers*, Wiley-VCH, Weinheim, 2010; (*f*) B. M. Rosen, C. J. Wilson, D. A. Wilson, M. Peterca, M. R. Imam and V. Percec, *Chem. Rev.*, 2009, **109**, 6275–6540.

7 (*a*) Z. S. Yoon, Y.-T. Chan, S. Li, G. R. Newkome and T. G. Goodson III, *J. Phys. Chem. B*, 2010, **114**, 11731–11736; (*b*) U. S. Schubert and C. Eschbaumer, *Angew. Chem., Int. Ed.*, 2002, **41**, 2892–2926; (*c*) J.-L. Wang, J. Yan, Z.-M. Tang, Q. Xiao, Y. Ma and J. Pei, *J. Am. Chem. Soc.*, 2008, **130**, 9952–9962; (*d*) B. Ventura, A. Barbieri, F. Barigelletti, S. Diring and R. Ziessel, *Inorg. Chem.*, 2010, **49**, 8333–8346.

8 (*a*) D. Armspach, M. Cattalini, E. C. Constable, C. E. Housecroft and D. Phillips, *Chem. Commun.*, 1996, 1823–1824; (*b*) U. S. Schubert, H. Hofmeier and G. R. Newkome, *Modern Terpyridine Chemistry*, Wiley-VCH, Weinheim, 2006; (*c*) A. Wild, A. Winter, F. Schlütter and U. S. Schubert, *Chem. Soc. Rev.*, 2010, **40**, 1459–1511; (*d*) U. S. Schubert, A. Winter and G. R. Newkome, *Terpyridine-based Materials*, Wiley-VCH, Weinheim, 2011.

9 (*a*) E. C. Constable and A. M. W. C. Thompson, *J. Chem. Soc., Chem. Commun.*, 1992, 617–619; (*b*) M. Osawa, M. Hoshino, S. Horiuchi and Y. Wakatsuki, *Organometallics*, 1999, **18**, 112–114.

10 (*a*) S. Sato, Y. Ishido and M. Fujita, *J. Am. Chem. Soc.*, 2009, **131**, 6064–6065; (*b*) W. Jiang, A. Schafer, P. C. Mohr and C. A. Schalley, *J. Am. Chem. Soc.*, 2010, **132**, 2309–2320; (*c*) J.-L. Wang, Y.-T. Chan, C. N. Moorefield, J. Pei, D. A. Modarelli, N. C. Romano and G. R. Newkome, *Macromol. Rapid Commun.*, 2010, **31**, 850–855.

11 J.-L. Wang, X. Li, X. Lu, Y.-T. Chan, C. N. Moorefield, C. Wesdemiotis and G. R. Newkome, *Chem.–Eur. J.*, 2011, **17**, 4830–4838.

12 (*a*) C. S. Hoaglund-Hyzer, A. E. Counterman and D. E. Clemmer, *Chem. Rev.*, 1999, **99**, 3027–3079; (*b*) S. Trimpin and D. E. Clemmer, *Anal. Chem.*, 2008, **80**, 9073–9083; (*c*) B. T. Ruotolo, J. L. P. Benesch, A. M. Sandercock, S. J. Hyung and C. V. Robinson, *Nat. Protoc.*, 2008, **3**, 1139–1152; (*d*) A. C. Joerger, S. Rajagopalan, E. Natan, D. B. Veprintsev, C. V. Robinson and A. R. Fersht, *Proc. Natl. Acad. Sci. U. S. A.*, 2009, **106**, 17705–17710; (*e*) K. Thalassinos, M. Grabenauer, S. E. Slade, G. R. Hilton, M. T. Bowers and J. H. Scrivens, *Anal. Chem.*, 2009, **81**, 248–254.

13 (*a*) Y.-T. Chan, X. Li, M. Soler, J. L. Wang, C. Wesdemiotis and G. R. Newkome, *J. Am. Chem. Soc.*, 2009, **131**, 16395–16397; (*b*) E. R. Brocker, S. E. Anderson, B. H. Northrop, P. J. Stang and M. T. Bowers, *J. Am. Chem. Soc.*, 2010, **132**, 13486–13494; (*c*) X. Li, Y.-T. Chan, G. R. Newkome and C. Wesdemiotis, *Anal. Chem.*, 2011, **83**, 1284–1290; (*d*) Y.-T. Chan, X. Li, J. Yu, G. A. Carri, C. N. Moorefield, G. R. Newkome and C. Wesdemiotis, *J. Am. Chem. Soc.*, 2011, **133**, 11967–11976.

14 J. Závada, M. Pánková, P. Holý and M. Tichý, *Synthesis*, 1994, 1132.

15 G. W. V. Cave and C. Raston, *J. Chem. Soc., Perkin Trans. 1*, 2001, 3258–3264.

16 T. Mutai, J.-D. Cheon, S. Arita and K. Araki, *J. Chem. Soc., Perkin Trans. 2*, 2001, 1045–1050.

17 I. P. Evans, E. A. Spencer and G. Wilkinson, *J. Chem. Soc., Dalton Trans.*, 1973, 204–209.

18 C. D. Shreiner, C. N. Moorefield, D. V. Reddy, T. J. Cho, D. K. Parker, F. R. Fronczek, S. R. Tummalapalli and G. R. Newkome, *J. Inorg. Organomet. Polym. Mater.*, 2005, **15**, 459–467.

19 J. K. McCusker, K. N. Walda, R. C. Dunn, J. D. Simon, D. Magde and D. N. Hendrickson, *J. Am. Chem. Soc.*, 1993, **115**, 298–307.

20 J.-L. Wang, Y. Zhou, Y. Li and J. Pei, *J. Org. Chem.*, 2009, **74**, 7449–7456.

21 C.-Q. Ma, M. Fonrodona, M. C. Schikora, M. M. Wienk, R. A. J. Janssen and P. Bäuerle, *Adv. Funct. Mater.*, 2008, **18**, 3323–3331.